Crystal Structure of a Novel Zinc-Binding ATP Sulfurylase from *Thermus thermophilus* HB8[†,‡]

Yuichi Taguchi,[§] Masakazu Sugishima,[§] and Keiichi Fukuyama*[,§,||]

Department of Biology, Graduate School of Science, Osaka University, 1-1 Machikaneyama, Toyonaka, Osaka 560-0043, Japan, and RIKEN Harima Institute/SPring-8, 1-1-1 Koto, Mikazuki-cho, Sayo-gun, Hyogo 679-5148, Japan

Received November 17, 2003; Revised Manuscript Received February 10, 2004

ABSTRACT: ATP sulfurylase (ATPS) is a ubiquitous enzyme that catalyzes the transfer of the adenylyl group from ATP to inorganic sulfate, producing adenosine 5′-phosphosulfate (APS) and pyrophosphate. The crystal structure of ATPS from *Thermus thermophilus* HB8 (TtATPS, 347 amino acid residues) in complex with APS was determined at 2.5 Å resolution. TtATPS is composed of three domains [domain I (residues 1−134), domain II (residues 135−290), and domain III (residues 291−347)], like the *Riftia pachyptila* symbiont ATPS, but lacks a fourth domain present in ATPSs from the yeast *Saccharomyces cerevisiae* and from the fungus *Penicillium chrysogenum*. TtATPS forms a dimer in the crystal, and the manner of subunit association is different from that observed in dimeric *R. pachyptila* symbiont ATPS and in the hexameric *S. cerevisiae* and *P. chrysogenum* ATPSs. APS is located in the active site of TtATPS, which contains several motifs (QXRN, HXXH, and GRD) conserved in ATPSs. Unexpectedly, TtATPS binds one metal ion per subunit in domain III. XAFS measurement of the crystal and the Bijvoet difference Fourier map unambiguously characterized the metal ion as a zinc ion. The zinc ion is tetrahedrally coordinated by Cys294, Cys297, Cys306, and His310, and could not be removed from the protein by treatment with EDTA. The zinc ion binding site is far from the active site. Because all four residues coordinated to the zinc ion are conserved in the ATPSs from thermophilic bacteria such as *Archaeoglobus fulgidus*, *Pyrococcus abyssi*, and *Sulfolobus solfataricus*, zinc ion chelation may contribute to the thermal stability of these ATPSs.

ATP sulfurylase (ATPS,[1] sulfate adenylyltransferase, EC 2.7.7.4) catalyzes the transfer of the adenylyl group from ATP to inorganic sulfate, yielding adenosine 5′-phosphosulfate (APS) and pyrophosphate (PP_i) (or the reaction of its reverse direction):

$$MgATP + SO_4^{2-} \rightarrow MgPP_i + APS \text{ (ATP sulfurylase)}$$

ATPS is a ubiquitous enzyme, although its physiological roles differ in organisms depending on their metabolic lifestyles. In many eukaryotes and bacteria, ATPS acts as the first enzyme in a cascade of proteins that activate inorganic sulfate (SO_4^{2-}) and incorporate it into organic compounds; APS produced by ATPS is subsequently phosphorylated at its 3′-position by APS kinase, yielding 3′-phosphoadenosine 5′-phosphosulfate (PAPS):

$$MgATP + APS \rightarrow PAPS + MgADP \text{ (APS kinase)}$$

PAPS serves as the sulfuryl donor for a variety of endogenous and exogenous chemicals by specific enzymes, e.g., sulfotransferase and heparan sulfate *N*-transferase (*1*−*3*). PAPS is also used for sulfate reduction; it serves as the substrate for an NADPH-dependent reduction that yields sulfite, which is further reduced for use in the biosynthesis of cysteine (*4*, *5*). Thus, APS and PAPS are used to produce sulfur-containing biological molecules. On the other hand, in the bacterial symbiont of the hydrothermal vent tubeworm *Riftia pachyptila*, ATPS acts to produce ATP and sulfate from APS and pyrophosphate (*6*). Indeed, the ATPS from this organism has high activity for the reverse reaction compared to the ATPSs which act as sulfate assimilators and sulfate reducers (*7*).

To date, crystal structures of ATPSs from the yeast *Saccharomyces cerevisiae* (ScATPS), from the fungus *Penicillium chrysogenum* (PcATPS), and from the bacterial symbiont of the tubeworm, *R. pachyptila*, have been reported (*8*−*12*). The crystal structures of these ATPSs and their complexes with various substrate analogues and inhibitors have provided a wealth of information about the mechanisms of catalysis and regulation of enzyme reactions. The ATPSs are oligomeric enzymes, and each subunit is composed of

[†] This work was supported in part by a Grant-in-Aid for Scientific Research on a Priority Area (Biological Machinery) to K.F. (11169223) and by a Grant-in-Aid for the National Project on Protein Structural and Functional Analyses from the Ministry of Education, Culture, Sports, Science, and Technology of Japan.

[‡] The atomic parameters and observed structure factors have been deposited in the RCSB Protein Data Bank (1V47).

* To whom correspondence should be addressed. Phone: +81-6-6850-5422. Fax: +81-6-6850-5425. E-mail: fukuyama@bio.sci.osaka-u.ac.jp.

[§] Osaka University.

[||] RIKEN Harima Institute/SPring-8.

[1] Abbreviations: ATPS, ATP sulfurylase; APS, adenosine 5′-phosphate; PAPS, 3′-phosphoadenosine 5′-phosphosulfate; TtATPS, ATP sulfurylase from *Thermus thermophilus* HB8; PcATPS, ATP sulfurylase from *Penicillium chrysogenum*; ScATPS, ATP sulfurylase from *Saccharomyces cerevisiae*; DdATPS, ATPS from *Desulfovibrio desulfuricans*; EDTA, ethylenediaminetetraacetate.

10.1021/bi036052t CCC: $27.50
Published on Web 03/19/2004

multiple domains. Each subunit of ScATPS and PcATPS has four domains (I−IV). The catalytic domain (domain II) has the ATP binding site, and the C-terminal domain (domain IV) is an APS kinase domain. The subunits of ScATPS and PcATPS are arranged as a dimer of trimers (D_3) to form a hexamer. Binding of PAPS to the C-terminal domain of PcATPS causes a significant conformational change which induces an allosteric transition (*10*). In contrast, *R. pachyptila* symbiont ATPS, which lacks the C-terminal domain contained in the yeast and fungal ATPSs, forms a dimer.

The genome of the Gram-negative eubacterium *Thermus thermophilus* HB8 contains an ORF (DDBJ/EMBL/GenBank accession number AB090277; project code 0343) encoding a probable ATPS (*13*). The amino acid sequence of this ORF is somewhat identical with the sequences of ScATPS (35%), PcATPS (35%), and *R. pachyptila* symbiont ATPS (30%) and contains conserved residues in domain II that are involved in catalysis. Probable ATPS from *T. thermophilus* HB8 (TtATPS) has 347 amino acid residues, in which the domain corresponding to the C-terminal domain (domain IV) of ScATPS and PcATPS is lacking, as in *R. pachyptila* symbiont ATPS. We have previously reported overproduction and purification of the probable TtATPS, which had high thermostability and probably existed in an oligomeric state different from those of ScATPS, PcATPS, and *R. pachyptila* symbiont ATPS (*14*). We also obtained crystals of TtATPS in complex with APS that are suitable for X-ray crystallographic analysis.

We present here the enzymatic characterization of this protein and the crystal structure of its complex with APS, revealing that TtATPS contains a novel zinc ion. We suggest that chelation of this metal ion is one way of acquiring thermostability of ATPSs in thermophilic bacteria.

EXPERIMENTAL PROCEDURES

Expression, Purification, and Crystallization of SeMet-Labeled Protein. Native TtATPS was expressed and purified as described previously (*14*). To express the protein labeled with selenomethionine (SeMet), *Escherichia coli* B834(DE3) cells carrying the expression plasmid were precultured in Luria-Bertani medium as used for expression of TtATPS at 37 °C for a few hours (until the beginning of the log phase was reached). The preculture was inoculated into LeMaster medium (*15*) containing SeMet with lactose as a carbon source and cultured at 37 °C for 24 h. The SeMet-labeled TtATPS was purified in the same manner used to purify the native TtATPS. The SeMet-labeled TtATPS in complex with APS was crystallized under the same conditions that were used for the TtATPS−APS complex (*14*).

TtATPS Enzymatic Assay. Molybdolysis and ATP synthesis were assayed according to the published procedures (*16*). All reactions were performed in 50 mM Tris-HCl (pH 8.0) at 37 °C. One unit of enzyme activity corresponds to 1 μmol of primary product formed per minute. Molybdolysis (MgATP + MoO_4^{2-} → $MgPP_i$ + AMP + MoO_4^{2-}) was assessed in a reaction coupled to an inorganic pyrophosphatase reaction. The reaction was started by addition of the enzyme; incubation was carried out for 30 min, and the reaction was stopped by addition of acetic acid. The phosphate that was produced was colored by adding ammonium molybdate, sodium ascorbate, and sulfuric acid and incubating the mixture for 20 min at room temperature. The quantity of phosphate was determined by measuring the absorbance at 660 nm. The stoichiometry is 2 mol of phosphate formed per mole of pyrophosphate formed. ATP synthesis ($MgPP_i$ + APS → MgATP + SO_4^{2-}) was assessed in a reaction coupled to hexokinase and glucose-6-phosphate dehydrogenase reactions. The reaction was started by adding APS. The quantity of NADH was continuously measured by the absorbance at 340 nm. The stoichiometry is 1 mol of NAD^+ reduced per mole of ATP formed. The thermal stability of TtATPS was also monitored by the ATP synthesis assay. TtATPS was incubated at 80 °C and then immediately cooled on ice. The ATP synthesis activity of each sample (incubation times of 0, 5, 10, 20, 40, and 60 min) was measured three times. The remaining activity of TtATPS was evaluated by the increment of the absorbance during the 1 min reaction.

Data Collection and Processing. The crystal of the SeMet-labeled complex was soaked for a few minutes in the cryoprotectant [15% polyethylene glycol 6000, 0.1 M MES (pH 6.0), 5 mg/mL APS, and 25% ethylene glycol] and then flash-cooled with a nitrogen gas stream at 100 K. X-ray diffraction data of the complex were collected with a MarCCD detector and synchrotron radiation at beamline 44B2 (SPring-8). The MAD data were collected to 2.8 Å resolution with an oscillation angle per frame of 1.5° at three wavelengths (peak of 0.9794 Å, edge of 0.9806 Å, and remote of 0.9000 Å). All data were processed with DENZO and SCALEPACK (*17*). The space group of the SeMet-labeled complex crystal is $P2_1$, like that of the native complex crystal (*14*). The asymmetric unit contains two complexes, for which the V_M (*18*) value is 3.49 $Å^3$/Da. Crystal data and the results of crystallographic measurements are given in Table 1.

Structure Determination. An initial attempt to determine the structure by the MAD method was unsuccessful; the selenium sites could not be determined by the difference Patterson map. The molecular replacement method was applied using the PcATPS monomer structure as the search model. The model of residues 27−387 was used, where the residues that are not identical in TtATPS were set to alanine. Cross-rotation function and translation search using CNS (*19*) gave two sets of solutions, and the resulting models packed nicely in the unit cell. The coordinates were used to calculate the phases, which were combined with the Bijvoet differences of the observed structure factors of SeTtATPS to calculate the difference Fourier map. The map showed five distinct peaks per subunit; four of the five peaks clearly corresponded to the selenium atoms of the four SeMet residues, and the fifth peak found in domain III was assumed to be a metal ion. This confirmed that the overall structure was correct; however, the model of several regions in domain III required substantial correction as judged from the $F_o - F_c$ map and improper stereochemical arrangement between the peptide segment and the metal ion. Thus, a less biased electron density map was prepared on the basis of the Bijvoet differences and the four selenium sites, where the dispersive data were ignored because they had little phasing power. The phases were improved by the density modification. The model was fitted to the map with the aid of the amino acid sequence using O (*20*). The structure was revised by alternately adjusting the model and simulated annealing refinement using the peak data of the SeMet form of TtATPS to 2.7 Å resolution. The bound APS and several water

Table 1: Data Collection and Refinement Statistics

Data Collection					
	SeMet-labeled TtATPS−APS complex			TtATPS−APS complex	
	peak	edge	remote	high remote	low remote
unit cell constants	$a = 68.8$ Å, $b = 61.4$ Å, $c = 129.4$ Å, $\beta = 96.2°$			$a = 68.8$ Å, $b = 61.2$ Å, $c = 128.6$ Å, $\beta = 95.4°$	
wavelength (Å)	0.9794	0.9806	0.9000	1.270	1.295
resolution (Å)	2.7	2.7	2.9	2.9	2.49
no. of measured reflections	225577	225429	135409	134310	207915
no. of unique reflections	29663	29702	24178	23855	37661
redundancy[a]	7.6 (7.2)	7.2 (7.1)	5.6 (5.6)	5.6 (5.7)	5.5 (5.2)
completeness (%)[a]	99.7 (100)	99.7 (100)	99.6 (100)	100 (100)	99.7 (97.1)
R_{merge} (%)[a,b]	7.5 (24.6)	7.3 (31.2)	8.5 (28.8)	6.0 (12.5)	6.1 (20.5)
$I/\sigma I$[a]	26.6 (7.7)	25.1 (5.6)	18.3 (5.8)	26.9 (9.6)	24.9 (8.0)

Refinement Statistics		
resolution range (Å)	20.0−2.49	
no. of unique reflections ($F > 0$)	37238	
R_{cryst}/R_{free} (%)[c]	21.9/26.9	
no. of protein/APS atoms[d]	5383/54	
no. of Zn^{2+} ions/Na^+ ions/Cl^- ions/waters[d]	2/4/5/164	
rms deviations from ideality		
bond lengths (Å)	0.006	
bond angles (deg)	1.32	
Ramachandran plots		
most favored (%)	90.6[e]	84.0[f]
additional allowed (%)	9.4[e]	15.2[f]
generously allowed (%)	0.0[e]	0.7[f]
disallowed (%)	0.0[e]	0.0[f]

[a] The values in parentheses are for the highest-resolution shell. [b] $R_{merge} = \sum_{hkl}\sum_i |I_i(hkl) - \langle I(hkl)\rangle| / \sum_{hkl}\sum_i I_i(hkl)$. [c] R_{free} was calculated for 10% of the reflections randomly excluded from the refinement. [d] Number in the asymmetric unit. [e] For molecule A. [f] For molecule B.

molecules were located in the $2F_o - F_c$ and $F_o - F_c$ maps and included in the subsequent refinement. The structure was refined using CNS (*19*) to R and R_{free} values of 23.8 and 28.0%, respectively. The structure of native TtATPS was determined by the molecular replacement method using the SeTtATPS model because the lack of isomorphism between these crystals was substantial.

Characterization of the Metal Ion and Refinement. From the peak heights in the Bijvoet difference map at a λ of 0.9794 Å and in the $2F_o - F_c$ map, four possibilities (zinc, nickel, cobalt, and iron) existed for the metal ion bound to TtATPS. XAFS of the native crystal was measured around each absorption edge of these metal ions. To confirm the XAFS measurement and to further investigate whether metal ions other than zinc ion partially occupy this site, X-ray diffraction data were collected at the high and low remote (1.270 and 1.295 Å) of the zinc absorption edge ($\lambda = 1.283$ Å).

The structure was further refined by incorporating the zinc ion and APS using the diffraction data ($\lambda = 1.295$ Å) of the native crystal. Alternating cycles of simulated annealing and model adjustment, including water picking, gave R and R_{free} values of 21.9 and 26.9%, respectively, using the diffraction data to 2.5 Å resolution. Refinement statistics are given in Table 2. The volume of the active pocket was calculated with CASTp (*21*) using a 1.4 Å probe. Domain IV was deleted in the models of ScATPS and PcATPS for calculation of the volume of the active pocket.

Measurement of the Zinc Content in TtATPS. The zinc content in TtATPS was analyzed with a Shimadzu AA-6400G atomic absorption spectrophotometer equipped with a GFA-6500 graphite furnace atomizer using commercially available metal standard solutions. To reduce the sensitivity of the zinc signal, inner gas flowed at a rate of 0.5 mL/min in ashing and atomizing procedures. The EDTA-treated form was prepared as follows. TtATPS was incubated with 50 mM EDTA on ice for 1 day and then dialyzed twice against Tris-HCl (pH 8.0) buffer. The dialysis buffer was pretreated with Chelating Resin (Hampton Research) to remove contaminating zinc ion. The dialysis membrane was washed with an EDTA solution and ddH_2O. Native TtATPS used in this measurement was also dialyzed against the same buffer. The protein concentration was determined by the Lowry assay using bovine serum albumin as a standard.

Table 2: Geometry around Zn^{2+} Ion

Distances to Zn^{2+} Ion (Å)		
	molecule A	molecule B
Cys294 Sγ	2.09	2.29
Cys297 Sγ	2.39	2.43
Cys306 Sγ	2.21	2.22
His310 Nδ	2.06	2.32

Coordination Angles (deg)		
	molecule A	molecule B
Cys294 Sγ−Zn^{2+}−Cys297 Sγ	113.9	113.1
Cys294 Sγ−Zn^{2+}−Cys306 Sγ	116.7	110.1
Cys294 Sγ−Zn^{2+}−His310 Nδ	110.5	109.9
Cys297 Sγ−Zn^{2+}−Cys306 Sγ	108.9	109.2
Cys297 Sγ−Zn^{2+}−His310 Nδ	102.9	104.3
Cys306 Sγ−Zn^{2+}−His310 Nδ	102.5	110.2

RESULTS AND DISCUSSION

Activity of TtATPS. The enzyme assays at 37 °C determined activities of 0.0056 unit/mg for molybdolysis and 1.61 units/mg [K_M(APS) = 40 μM] for ATP synthesis, confirming that this gene product indeed has ATP sufurylase activity. The activity of TtATPS for molybdolysis, however, is markedly low compared with the activities of other ATPSs:

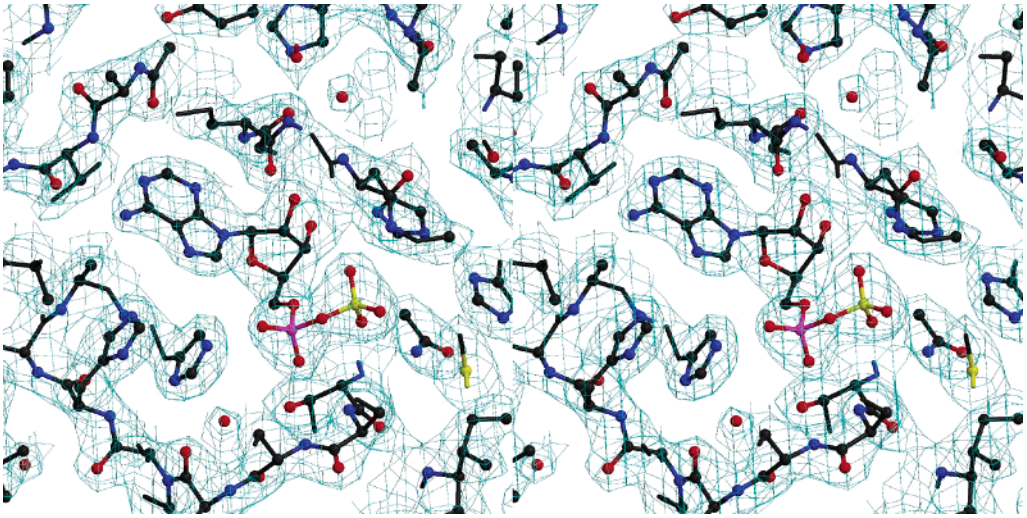

FIGURE 1: Stereoview of the $2F_o - F_c$ map around the active site of TtATPS. The map contoured at 1.2σ is superimposed on the refined model.

rat ATPS (14.2 units/mg) (*22*), *R. pachyptila* symbiont ATPS (65 units/mg) (*7*), and *Aquifex aerolicus* ATPS (3.6 units/mg) (*23*). In contrast, the activity of TtATPS for ATP synthesis is comparable to the activity of rat ATPS (12.5 units/mg) (*22*), *R. pachyptila* symbiont ATPS (370 units/mg) (*7*), and *A. aerolicus* ATPS (13.1 units/mg) (*23*). Half of the ATP synthesis activity of TtATPS was retained after incubation at 80 °C for 40 min. The remarkably high activity of *R. pachyptila* symbiont ATPS for ATP synthesis is proposed to be due to the fact that this organism uses this enzyme to acquire ATP from APS. The low observed activity of TtATPS may be due to the temperature (37 °C) used for the enzymatic activity assay.

Overall Structure. A $2F_o - F_c$ map around the bound APS is shown in Figure 1. A schematic drawing of TtATPS in complex with APS is shown in Figure 2a. TtATPS is composed of three domains [domain I (residues 1−134), domain II (residues 135−290), and domain III (residues 291−347)]. Superimposition of TtATPS and PcATPS is shown in Figure 2b. TtATPS, like *R. pachyptila* symbiont ATPS, lacks the fourth domain present in ScATPS and PcATPS. The primary and tertiary structures of this domain are similar to those of APS kinase, the enzyme which catalyzes phosphorylation of the 3′-OH group of APS to produce 3′-adenosine 5′-phosphosulfate (PAPS); ATPS and APS kinase are fused in eukaryotic ATPSs such as PcATPS and ScATPS to efficiently channel APS into the adjacent kinase reaction. It is unknown, however, whether *T. thermophilus* has an APS kinase.

The peptide chain folding of domains I−III and the orientation of these domains in TtATPS are similar to those in PcATPS. Domain I consists of a β-sheet comprising five β-strands with four α-helices on its one side, and domain II consists of a central β-sheet of five parallel β-strands with five flanking α-helices. APS binds primarily to domain II. Domain III has an elongated shape and covers one side of domain II and the bound APS. A characteristic of domain III of TtATPS is the location of the zinc ion (see below). As shown in Figure 2b, TtATPS lacks domain IV like *R. pachyptila* symbiont ATPS (*12*). Compared with ScATPS, two N-terminal helices (H1 and H2) and a loop in domain II (S12−H12 loop) are lacking in TtATPS. This may contribute to the thermostability of TtATPS (*24*, *25*).

The intermolecular contacts in TtATPS are shown in Figure 2c. TtATPS appears to form a dimer, but its contact surface is narrow (1045 Å^2). In gel chromatography, TtATPS eluted at a retention time corresponding to ∼55.5 kDa, which is between the expected values for a monomer and a dimer (*14*). This suggests that TtATPS does not form a stable dimer. The manner of the intermolecular interaction of TtATPS is distinct from that of *R. pachyptila* symbiont ATPS, a dimeric enzyme, with a contact surface of 1574 Å^2. It also differs from any of the intermolecular interactions in hexameric PcATPS and ScATPS.

Structure of the Active Site and the Catalytic Mechanism. This structural analysis clearly located the bound APS. A close-up view around the APS is shown in Figure 3. The surface of TtATPS around the APS is positively charged (not shown). The sulfate moiety of APS interacts with Gln162, Arg164, and Ala260, the phosphate moiety with Thr163 and His171 and with Asn165 via a water molecule, the sugar moiety with Gly256, Arg257, and His259 and with Gln162 and Leu254 via a water molecule, and the adenine moiety with Val291 and Ile317. The residues involved in APS binding are highly conserved in ATPSs. Indeed, the manner of APS binding in TtATPS is similar to that in ScATPS and PcATPS, although His204 of ScATPS (corresponding to His171 of TtATPS) does not interact with APS. The active site pocket of the TtATPS−APS complex is more compact than the active site pockets of other ATPS−APS complexes (1241.3 Å^3 for TtATPS, 2092.9 Å^3 for ScATPS, and 2296.5 Å^3 for PcATPS). The shrinkage of the active site is primarily achieved by the decline of domain III, which induces closure of the loop segment (Thr315−Met319) (Figure 4). Zinc binding and/or dimer interaction may contribute to the tight active site of TtATPS. A similar difference of compactness of the active cleft is also seen in glutamate dehydrogenases from the hyperthermophilic archaeon *Pyrococcus furiosus* and from the mesophilic bacterium *Clostridium symbiosum* (*26*). A compact active site would indicate adaptation to a hot environment: tightness of the active site would contribute to the thermostablity of the active site (*24*). Increasing the

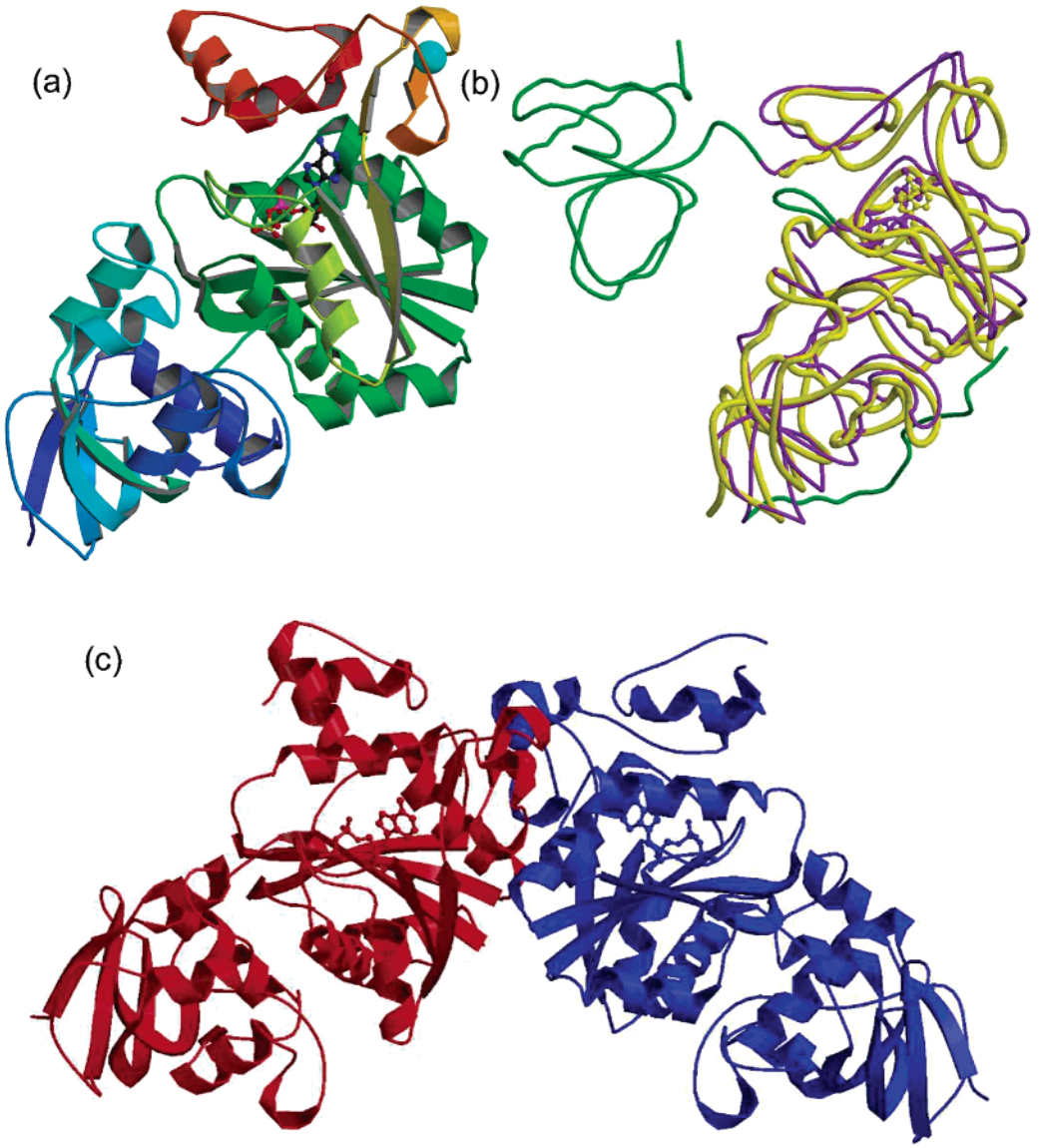

FIGURE 2: Structure of TtATPS. (a) Ribbon drawing of TtATPS with APS (ball-and-stick model) and Zn^{2+} ion (blue sphere). The N-terminus is blue, and the C-terminus is red, with intermediate colors following the distance in sequence from the N-terminus. (b) Superimposition of TtATPS (yellow) and ScATPS (purple and green). Green shows segments which are absent in TtATPS. (c) Protein−protein interactions in TtATPS. Intermolecular distances are as follows: Tyr173 OH−Glu180 Oϵ, 2.5/2.7 Å; Arg176 Nη−Cys297 Sγ, 3.3/3.4 Å; Arg176 Nη−Thr305 O, 2.9/3.2 Å; Glu180 Oϵ−Ser302 Oγ, 2.6/2.9 Å; Asp214 O−His310 Nϵ, 2.7/3.2 Å; Arg220 Nη−Arg304 O, 2.4 Å; Leu296 O−Arg338 Nη, 3.2/3.4 Å; Cys297 O−Arg338 Nη, 2.8 Å; Thr305 Oγ−H_2O−Arg176 Nη, 3.0 and 3.2 Å, respectively; Lys208 O−H_2O−Glu180 Oϵ, 2.8 and 3.2 Å, respectively; and Glu180 O−H_2O−Lys287 O, 2.5 and 3.0 Å, respectively.

temperature would induce flexibility of the loop located at the active site entrance and enhance the activity of TtATPS.

The crystal structures of the binary ScATPS product complex with APS and the ternary product complex, including pyrophosphate, led to a proposal of the mechanism by which ATP and sulfate are trapped by ScATPS (*9*). The locations of the active residues and the residues that interacted with substrates and/or products are highly conserved between TtATPS and ScATPS. The γ- and β-phosphates of ATP interact with His201 and His204, respectively (which correspond to His168 and His171 in TtATPS, respectively), and the α-phosphate interacts with Thr196 and Gln198 in a way similar to the way APS interacts in TtATPS and ScATPS. The sulfate ion in this model occupies the site corresponding to the sulfate moiety of APS in TtATPS and that in ScATPS. The ATP substrate may be inserted in the small cavity near APS in TtATPS by repelling out a water molecule, where His168 and His171 residues serve to bind ATP. The sulfate substrate may bind to a similar site like the sulfate moiety of APS in TtATPS, and carry out a nucleophilic attack on the α-phosphate of the bound ATP, as has been proposed for ScATPS (*8*, *9*).

Coordination of the Zinc Ion. XAFS measured near each absorption edge of the possible metal ions gave a notable signal only at the absorption edge of zinc ion (Figure 5a). Furthermore, the Bijvoet difference Fourier map based on the data at a λ of 1.270 Å showed a significant peak at the metal site, whereas the peak height based on the data at a λ of 1.295 Å was remarkably low (Figure 5b). This shows that the site exclusively binds zinc ion. The analyses of the atomic absorption and protein concentration showed that the molar ratio of zinc to protein in solution was 0.89 ± 0.05; zinc ion is likely to be bound to the protein with a 1:1 ratio considering the limitation of the protein assay using bovine

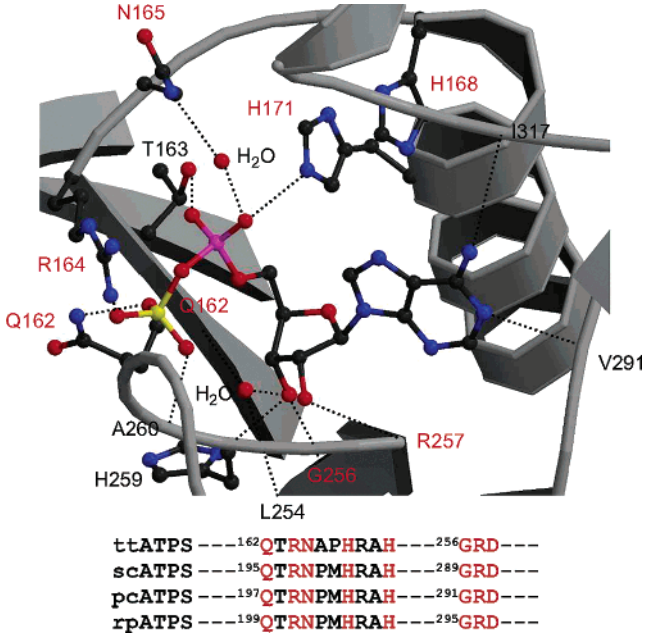

FIGURE 3: Close-up view of the active site of the TtATPS−APS complex. APS and the side chains of the residues interacting with APS are shown as a ball-and-stick model. The labels of the conserved residues are shown in red. The interatomic distances involved in APS binding are as follows: Gln162 Nϵ−O3B, 2.8/2.9 Å; Gln162 N−H_2O−O3*, 2.8 and 3.2 Å, respectively; Thr163 Oγ−O1A, 2.7/3.3 Å; Arg164 Nη−O1B, 2.7/2.8 Å; Asn165 Nδ−H_2O−O2A, 2.7 and 2.6 Å, respectively; His171 Nϵ−O2A, 2.8/3.2 Å; Leu254 O−H_2O−O3*, 2.8 and 3.2 Å, respectively; Gly256 N−O3*, 3.0/3.1 Å; Arg257 O−O2*, 2.7/2.9 Å; His259 Nδ−O3*, 2.8/2.9 Å; Ala260 N−O2B, 2.7/2.8 Å; Val291 N−N1, 2.9/3.0 Å; and Ile317 O−N6, 2.9/3.2 Å.

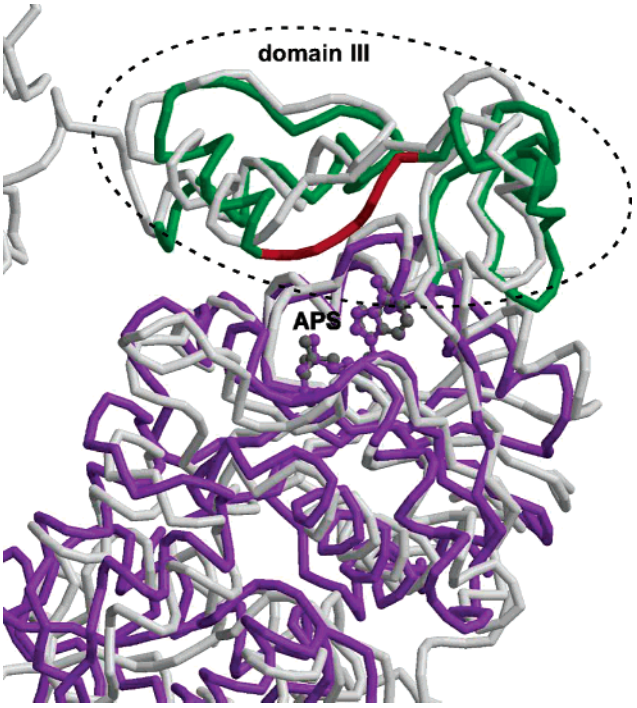

FIGURE 4: Comparison of the active sites of TtATPS and ScATPS. A Cα trace of ScATPS (gray) was superimposed on that of TtATPS [domain III (green), Thr315−Met319 (red), and other (purple)] to minimize the deviation of the APS molecules. APS (purple) and zinc (green) were shown as ball-and-stick and CPK models, respectively.

serum albumin as the standard. In addition, the ratio was changed little by incubation with 50 mM EDTA for 1 day, showing that the zinc ion is not released from TtATPS. No zinc ion was artificially added to any of the solutions used for purification and crystallization of TtATPS and its SeMet form (*14*). Zinc ion from the culture medium or in *E. coli* was probably bound to the protein.

The zinc ion is coordinated by four atoms: the Sγ atoms of Cys294, Cys297, and Cys306 and the Nδ atom of His310. The coordination geometry is close to tetrahedral (Table 2).

TtATPS is the first ATPS that has been clearly demonstrated to bind zinc ion. Although it was reported that ScATPS bound cadmium ions added for crystallization, this observation differs from that with TtATPS in that the cadmium ions bound to the surface of the ScATPS subunits (*9*). Gavel *et al.* (*27*) reported, on the basis of EXAFS and EPR studies, that ATPSs from *Desulfovibrio gigas* and *Desulfovibrio desulfuricans* bound either cobalt or zinc ion through three cysteines and one histidine. The draft genome sequence of *D. desulfuricans* G20 was recently determined, and its ATPS homologue was annotated (accession number ZP_00129812). The amino acid sequence of this ATPS homologue shows

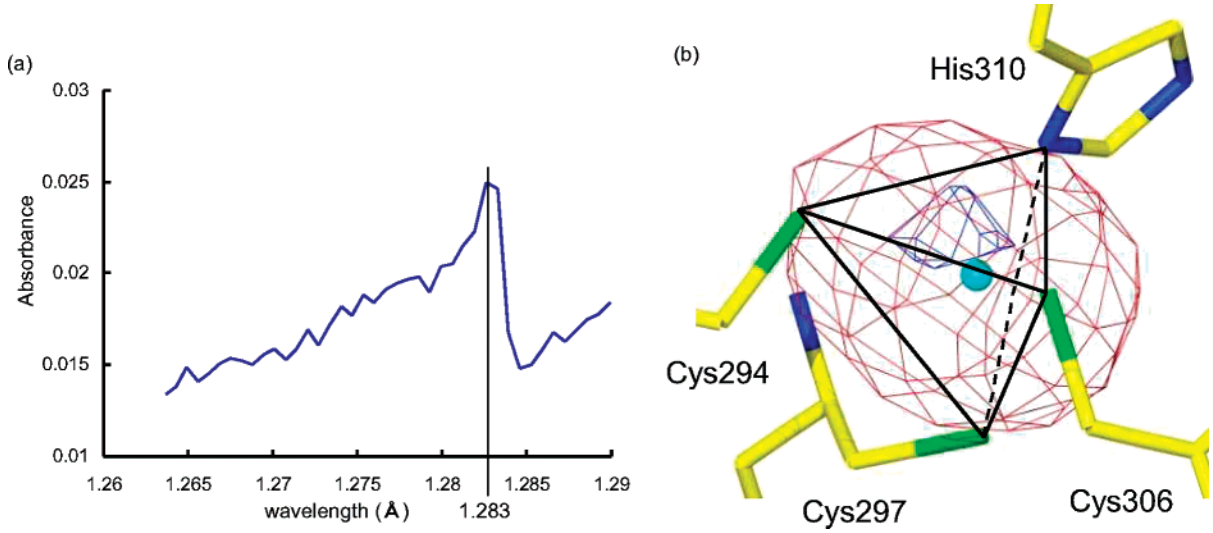

FIGURE 5: Characterization of the bound metal ion. (a) XAFS measurement near the absorption edge of zinc ion. (b) Bijvoet difference maps based on the diffraction data at a λ of 1.270 Å (red) and at a λ of 1.295 Å (blue). The contour level is 7σ.

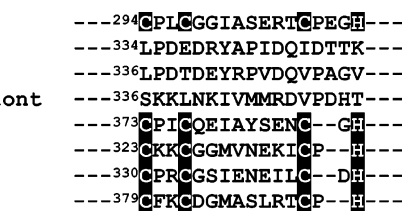

FIGURE 6: Sequence comparison of zinc binding segments in ATPSs. Initial multiple-sequence alignment was determined using ClustalW and the BLOSUM64 substitution scoring matrix with "open-gap" and "extend-gap" penalties of 10 and 0.05. Minor manual adjustments were done for better fitting. The residues involved in zinc binding in TtATPS and the putative metal-binding residues in the three thermophilic bacteria and *D. desulfuricans* G20 have a black background.

that it lacks domain IV, as does TtATPS. The three cysteines and one histidine involved in zinc binding in TtATPS are conserved in ATPS from *D. desulfuricans* (DdATPS), although two residues are deleted between the third cysteine and the histidine, suggesting that these residues in DdATPS bind zinc or cobalt ion. However, DdATPS forms a homotrimer (*27*), unlike TtATPS, and the shrinkage of the active site caused by the dimer interaction as seen in TtATPS would not occur in DdATPS.

Role of the Zinc Ion in TtATPS. The zinc ion is located in the N-terminal half of domain III, immediately after domain II. The distances from the ion to the adenine ring of the bound APS and to His171 are 14 and 17 Å, respectively. The zinc ion is tightly and selectively bound to this site. Domain III covers the active site of TtATPS, and the adenine moiety of the bound APS interacts with Val291 and Ile317. The zinc-binding region appears to be a hinge between domains II and III and is also involved in protein−protein interactions (Figure 2c). Presumably, the zinc ion contributes to holding the conformation of this region in the correct orientation. If domain III, which constitutes a part of the active site, were allowed to move more readily, the correct orientation of domains II and III would collapse at elevated temperatures.

Alignment of the known sequences of ATPSs has revealed that ATPS from thermophilic bacteria such as *Archaeoglobus fulgidus*, *Pyrococcus abyssi*, and *Sulfolobus solfataricus* have the characteristic zinc-binding motif seen in TtATPS (Figure 6). Although there is only one residue between the third cysteine and the histidine residues in some of these ATPSs (there are three residues between the cysteine and histidine residues in TtATPS), the TtATPS structure suggests that deletion of two residues will not affect the chelation of zinc ion. We hypothesize that ATPSs from thermophilic bacteria acquire thermostability by chelating metal ions such as zinc ion. Indeed, thermostability acquired by zinc binding is suggested in such proteins as ferredoxin (*28*), α-amylase (*29*), proteinase (*30*), tRNA synthetase (*31*), pyruvate carboxylase (*32*), and lipase (*33*).

ACKNOWLEDGMENT

We thank Drs. Jun Hoseki, Noriko Nakagawa, Emi Ishido, and Seiki Kuramitsu of RIKEN Harima Institute for preparation of the native and SeMet-labeled TtATPS and Drs. Toshihide Okajima and Katsuyuki Tanizawa for their help with the atomic absorption analysis. We also thank Dr. Yoshimitsu Kakuta of Kyushu University (Fukuoka, Japan), Drs. Taiji Matsu and Takaaki Hikima of RIKEN, and Drs. Masahide Kawamoto and Hisanobu Sakai of JASRI (Sayo, Japan) for their aid with data collection using the synchrotron radiation at SPring-8.

REFERENCES

1. Weinshilboum, R. M., Otterness, D. M., Aksoy, I. A., Wood, T. C., Her, C., and Raftogianis, R. B. (1997) Sulfation and sulfotransferases 1: Sulfotransferase molecular biology: cDNAs and genes, *FASEB J. 11*, 3−14.
2. Kakuta, Y., Pedersen, L. G., Carter, C. W., Negishi, M., and Pedersen, L. C. (1997) Crystal structure of estrogen sulphotransferase, *Nat. Struct. Biol. 4*, 904−908.
3. Kakuta, Y., Sueyoshi, T., Negishi, M., and Pedersen, L. C. (1999) Crystal structure of the sulfotransferase domain of human heparan sulfate N-deacetylase/N-sulfotransferase 1, *J. Biol. Chem. 274*, 10673−10676.
4. Marzluf, G. A. (1997) Molecular genetics of sulfur assimilation in filamentous fungi and yeast, *Annu. Rev. Microbiol. 51*, 73−96.
5. Coughtrie, M. W., Sharp, S., Maxwell, K., and Innes, N. P. (1998) Biology and function of the reversible sulfation pathway catalysed by human sulfotransferases and sulfatases, *Chem.-Biol. Interact. 109*, 3−27.
6. Cavanaugh, C. M., Gardiner, S. L., Jones, M. L., Jannasch, H. W., and Waterbury, J. B. (1981) Prokaryotic cells in the hydrothermal vent tubeworm *Riftia pachyptila* Jones: possible chemoautotrophic symbionts, *Science 213*, 340−342.
7. Renosto, F., Martin, R. L., Borrell, J. L., Nelson, D. C., and Segel, I. H. (1991) ATP sulfurylase from trophosome tissue of *Riftia pachyptila* (hydrothermal vent tube worm), *Arch. Biochem. Biophys. 290*, 66−78.
8. Ullrich, T. C., and Huber, R. (2001) The complex structures of ATP sulfurylase with thiosulfate, ADP and chlorate reveal new insights in inhibitory effects and the catalytic cycle, *J. Mol. Biol. 313*, 1117−1125.
9. Ullrich, T. C., Blaesse, M., and Huber, R. (2001) Crystal structure of ATP sulfurylase from *Saccharomyces cerevisiae*, a key enzyme in sulfate activation, *EMBO J. 20*, 316−329.
10. MacRae, I. J., Segel, I. H., and Fisher, A. J. (2002) Allosteric inhibition via R-state destabilization in ATP sulfurylase from *Penicillium chrysogenum*, *Nat. Struct. Biol. 9*, 945−949.
11. MacRae, I. J., Segel, I. H., and Fisher, A. J. (2001) Crystal structure of ATP sulfurylase from *Penicillium chrysogenum*: insights into the allosteric regulation of sulfate assimilation, *Biochemistry 40*, 6795−6804.
12. Beynon, J. D., MacRae, I. J., Huston, S. L., Nelson, D. C., Segel, I. H., and Fisher, A. J. (2001) Crystal structure of ATP sulfurylase from the bacterial symbiont of the hydrothermal vent tubeworm *Riftia pachyptila*, *Biochemistry 40*, 14509−14517.
13. Yokoyama, S., Hirota, H., Kigawa, T., Yabuki, T., Shirouzu, M., Terada, T., Ito, Y., Matsuo, Y., Kuroda, Y., Nishimura, Y., Kyogoku, Y., Miki, K., Masui, R., and Kuramitsu, S. (2000) Structural genomics projects in Japan, *Nat. Struct. Biol. 7* (Suppl.), 943−945.
14. Taguchi, Y., Hoseki, J., Kakuta, Y., and Fukuyama, K. (2003) Overproduction, crystallization and preliminary X-ray diffraction analysis of probable ATP sulfurylase from *Thermus thermophilus* HB8, *Acta Crystallogr. D59*, 1645−1647.
15. LeMaster, D. M., and Richards, F. M. (1985) ^{1}H-^{15}N heteronuclear NMR studies of *Escherichia coli* thioredoxin in samples isotopically labeled by residue type, *Biochemistry 24*, 7263−7268.
16. Segel, I. H., Renosto, F., and Seubert, P. A. (1987) Sulfate-activating enzymes, *Methods Enzymol. 143*, 334−349.
17. Otwinowski, Z., and Minor, W. (1997) Processing of X-ray Diffraction Data Collected in Oscillation Mode, *Methods Enzymol. 276*, 307−326.
18. Matthews, B. W. (1968) Solvent content of protein crystals, *J. Mol. Biol. 33*, 491−497.
19. Brünger, A. T., Adams, P. D., Clore, G. M., DeLano, W. L., Gros, P., Grosse-Kunstleve, R. W., Jiang, J. S., Kuszewski, J., Nilges, M., Pannu, N. S., Read, R. J., Rice, L. M., Simonson, T., and Warren, G. L. (1998) Crystallography & NMR system: A new software suite for macromolecular structure determination, *Acta Crystallogr. D54*, 905−921.
20. Jones, T. A., Zou, J. Y., Cowan, S. W., and Kjeldgaard, M. (1991) Improved methods for building protein models in electron density

maps and the location of errors in these models, *Acta Crystallogr. A47*, 110−119.
21. Liang, J., Edelsbrunner, H., Fu, P., Sudhakar, P. V., and Subramaniam, S. (1998) Analytical shape computation of macromolecules: I. Molecular area and volume through alpha shape, *Proteins: Struct., Funct., Genet. 33*, 1−17.
22. Yu, M., Martin, R. L., Jain, S., Chen, L. J., and Segel, I. H. (1989) Rat liver ATP-sulfurylase: purification, kinetic characterization, and interaction with arsenate, selenate, phosphate, and other inorganic oxyanions, *Arch. Biochem. Biophys. 269*, 156−174.
23. Hanna, E., MacRae, I. J., Medina, D. C., Fisher, A. J., and Segel, I. H. (2002) ATP sulfurylase from the hyperthermophilic chemolithotroph *Aquifex aeolicus*, *Arch. Biochem. Biophys. 406*, 275−288.
24. Kumar, S., and Nussinov, R. (2001) How do thermophilic proteins deal with heat? *Cell. Mol. Life Sci. 58*, 1216−1233.
25. Russell, R. J., Ferguson, J. M., Hough, D. W., Danson, M. J., and Taylor, G. L. (1997) The crystal structure of citrate synthase from the hyperthermophilic archaeon *Pyrococcus furiosus* at 1.9 Å resolution, *Biochemistry 36*, 9983−9994.
26. Kumar, S., Ma, B., Tsai, C. J., and Nussinov, R. (2000) Electrostatic strengths of salt bridges in thermophilic and mesophilic glutamate dehydrogenase monomers, *Proteins: Struct., Funct., Genet. 38*, 368−383.
27. Gavel, O. Y., Bursakov, S. A., Calvete, J. J., George, G. N., Moura, J. J., and Moura, I. (1998) ATP sulfurylases from sulfate-reducing bacteria of the genus *Desulfovibrio*. A novel metalloprotein containing cobalt and zinc, *Biochemistry 37*, 16225−16232.
28. Fujii, T., Hata, Y., Wakagi, T., Tanaka, N., and Oshima, T. (1996) Novel zinc-binding centre in thermoacidophilic archaeal ferredoxins, *Nat. Struct. Biol. 3*, 834−837.
29. Savchenko, A., Vieille, C., Kang, S., and Zeikus, J. G. (2002) *Pyrococcus furiosus* α-amylase is stabilized by calcium and zinc, *Biochemistry 41*, 6193−6201.
30. Coolbear, T., Whittaker, J. M., and Daniel, R. M. (1992) The effect of metal ions on the activity and thermostability of the extracellular proteinase from a thermophilic *Bacillus*, strain EA.1, *Biochem. J. 287*, 367−374.
31. Kohda, D., Yokoyama, S., and Miyazawa, T. (1984) Thermostable valyl-tRNA, isoleucyl-tRNA and methionyl-tRNA synthetases from an extreme thermophile *Thermus thermophilus* HB8: protein structure and Zn^{2+} binding, *FEBS Lett. 174*, 20−23.
32. Libor, S., Sundaram, T. K., Warwick, R., Chapman, J. A., and Grundy, S. M. (1979) Pyruvate carboxylase from a thermophilic *Bacillus*: some molecular characteristics, *Biochemistry 18*, 3647−3653.
33. Tyndall, J. D., Sinchaikul, S., Fothergill-Gilmore, L. A., Taylor, P., and Walkinshaw, M. D. (2002) Crystal structure of a thermostable lipase from *Bacillus stearothermophilus* P1, *J. Mol. Biol. 323*, 859−869.

BI036052T